# Static friction boost in edge-driven incommensurate contacts

Davide Mandelli,[1,*] Roberto Guerra,[2] Wengen Ouyang,[1] Michael Urbakh,[1] and Andrea Vanossi[3,4]

[1]*Department of Physical Chemistry, School of Chemistry, The Raymond and Beverly Sackler Faculty of Exact Sciences and The Sackler Center for Computational Molecular and Materials Science, Tel Aviv University, Tel Aviv 6997801, Israel*

[2]*Center for Complexity and Biosystems, Department of Physics, University of Milan, 20133 Milan, Italy*

[3]*CNR-IOM Democritos National Simulation Center, Via Bonomea 265, 34136 Trieste, Italy*

[4]*International School for Advanced Studies (SISSA), Via Bonomea 265, 34136 Trieste, Italy*

(Received 16 February 2018; published 27 April 2018)

We present a numerical investigation of the size scaling of static friction in incommensurate two-dimensional contacts performed for different lateral loading configurations. Results of model simulations show that both the absolute value of the force $F_s$ and the scaling exponent $\gamma$ strongly depend on the loading configuration adopted to drive the slider along the substrate. Under edge loading, a sharp increase of static friction is observed above a critical size corresponding to the appearance of a localized commensurate dislocation. Noticeably, the existence of sublinear scaling, which is a fingerprint of superlubricity, does not conflict with the possibility to observe shear-induced localized commensurate regions at the contact interface. Atomistic simulations of gold islands sliding over graphite corroborate these findings, suggesting that similar elasticity effects should be at play in real frictional contacts.

DOI: 10.1103/PhysRevMaterials.2.046001

## I. INTRODUCTION

Sliding friction phenomena abound in nature, spanning, in disparate areas, vastly different scales of length, time, and energy [1]. However, despite their fundamental and technological importance, several key physical aspects of mechanical dissipative dynamics are not yet fully understood. This is mostly due to the complexity of highly out-of-equilibrium nonlinear processes occurring across a buried sliding interface [2]. Quite recently, new avenues of research are being pursued and new discoveries are being made especially at the microscopic scales [3,4]. In particular, dry solid/solid contacts displaying extremely low values of static and kinetic friction are attracting more and more attention due to their great physical and technological interest, e.g., to significantly reduce dissipation and wear in mechanical devices functioning at various scales. Unlike standard lubricants, solid lubrication arises from incommensurability of rigid interfaces causing effective cancellation of interfacial interactions. This phenomenon, often termed structural superlubricity, has been demonstrated in a number of experiments at nanoscales and microscales [5–19], yet its robustness and its upscale to the macroscopic world remain a challenge. The conditions of the persistence of superlubricity and the mechanisms of its failure are therefore cast as key questions to be addressed at both fundamental and technological levels.

Even in clean wearless friction experiments with perfect atomic structures the interface elasticity itself may hinder superlubricity by introducing new energy dissipation channels [20–23]. Recently, elasticity effects in contact area scaleup have shown to be critical for the breaking of ultralow frictional states when the contact size exceeds the core width of interfacial dislocations in crystalline interfaces [21]. Experimental evidences have been provided by measuring the sliding friction force of amorphous antimony particles on $MoS_2$ [24]. Again in connection to elasticity, the way that a driving local stress is applied to a slider, as typically occurs in proximal-probe nanomanipulation measurements, is expected to influence its tribological response as well. Indeed, within the idealized framework of a simple one-dimensional (1D) edge-driven Frenkel-Kontorova (FK) model [22,23], the abrupt occurrence of a striking boost in the dissipated energy during sliding (kinetic friction) has been observed above a critical contact length.

In this study, we consider two-dimensional (2D) superlubric elastic contacts, where even in the absence of defects a static friction arises due to finite-size edge effects [25]. In order to unveil the driving-induced mechanisms leading to the substantial elimination of superlubricity in a tribologically meaningful 2D geometry, we consider a FK-type modeling, highlighting the frictional phenomenology, and a comparative, more realistic, adsorbate/substrate atomistic simulation approach, mimicking the frictional interface of gold islands deposited on graphite. We found that the magnitude of the static friction and its scaling with the contact area strongly depend on the external lateral loading configuration. Large differences in the static friction observed between edge and uniform driving are tightly linked to the preslip strain distribution at the frictional interface. In particular, load-induced formation of localized commensurate regions can add to the edge contribution causing a sharp increase of the static friction force.

## II. FK MODELING AND RESULTS

### A. System and method

In our 2D FK model schematically sketched in Fig. 1(a), pointlike particles of mass $m$ form a square lattice of period

*Corresponding author: davidem@post.tau.ac.il

 

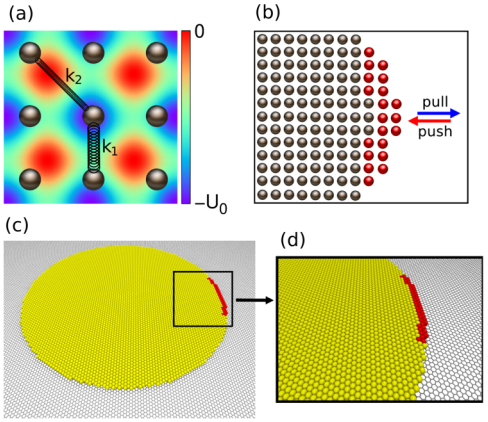


FIG. 1. (a) The 2D FK model adopted in simulations: a harmonic square lattice of identical point-mass particles interacting with a mismatched square substrate potential of strength $U_0$. (b) Schematics of the edge of a circular island in the 2D FK model, showing in red the particles to which the external force is applied during the edge-driving pulling/pushing protocols. (c) A circular gold island deposited over a graphene monolayer used in the atomistic simulations. (d) Detail of the region where the external force is applied during the edge-driving protocols (red atoms).

$a$. Each particle interacts with its four nearest neighbors via a potential

$$V_1(r_{ij}) = \begin{cases} \frac{k_1}{2}(r_{ij}-a)^2 & \text{if } r_{ij} > R_{\text{cut}}, \\ \alpha + \beta/r_{ij}^{12} & \text{if } r_{ij} \leqslant R_{\text{cut}}, \end{cases} \tag{1}$$

where $r_{ij} = |\mathbf{r}_i - \mathbf{r}_j|$ is the distance between particle $i$ and particle $j$. To get a closer description of a solid-state system, we introduced a cutoff distance $R_{\text{cut}}$, below which the interaction turns from harmonic to purely repulsive. The latter term models the Pauli repulsive forces between electron clouds of real atoms. The constants $\alpha$ and $\beta$ are chosen to ensure the continuity of $V_1(r)$ up to its first derivative at $r = R_{\text{cut}}$. The isostatic instability under shear forces of the square lattice is eliminated by including a second harmonic term accounting for the interactions between next-nearest neighbors:

$$V_2(r_{ij}) = \frac{k_2}{2}(r_{ij} - l_{\text{next}})^2, \tag{2}$$

where $l_{\text{next}} = a\sqrt{2}$ is the next-nearest-neighbor equilibrium distance, and the spring constant $k_2$ is chosen to give $k_1/k_2 = 2$, resulting in a 2D Poisson's ratio of $\sigma_{2D} = \frac{1}{3}$. Values adopted to perform the simulations are $a = 1$, $m = 1$, $R_{\text{cut}} = 0.85$, $k_1 = 10$, $k_2 = 5$.

A rigid crystalline substrate is modeled as a two-dimensional periodic potential of square symmetry, strength $U_0$, and periodicity $\lambda_{\text{sub}}$:

$$U(\mathbf{r_i}) = -\frac{U_0}{4}\left(2 + \cos\frac{2\pi x_i}{\lambda_{\text{sub}}} + \cos\frac{2\pi y_i}{\lambda_{\text{sub}}}\right). \tag{3}$$

We used $\lambda_{\text{sub}} = (1+\sqrt{5})/3 \approx 1.08$, resulting in an overdense interface, where the particle density is larger than the density of substrate potential minima. We chose a value of $U_0 = 0.075$ corresponding to an interfacial stiffness $U_0\pi^2/\lambda_{\text{sub}}^2 \approx 0.6$, which is more than one order of magnitude smaller than the internal stiffness $k_1 = 10$ of the monolayer, ensuring that the system is well within the superlubric regime. This is usually the case in nanomanipulation experiments [11,12,26]. This condition has been carefully checked in our model by measuring the static friction force of infinite monolayers in periodic boundary conditions, as detailed in Sec. S1 of Supplemental Material (SM) [27]. Together with the geometrical lattice mismatch, the ratio of the internal and interfacial stiffnesses is directly related to the characteristic core width $b_{\text{core}}$ of interfacial edge dislocations. This parameter was introduced to define a critical contact size above which elasticity becomes important and leads to local locking into the commensurate state [21]. For our 2D FK system, we estimated $b_{\text{core}} \approx 68\ a$ (see Sec. S2 of SM [27] for details).

At rest, the total energy of a system of $N_p$ particles is

$$E(\{\mathbf{r}_i\}) = \sum_{i=1}^{N_p} U(\mathbf{r_i}) + \sum_{\langle i,j\rangle} V_1(r_{ij}) + \sum_{\langle i,j\rangle_{\text{next}}} V_2(r_{ij}), \tag{4}$$

where $\langle i,j\rangle$ and $\langle i,j\rangle_{\text{next}}$ indicate summations over all distinct nearest- and next-nearest-neighbor pairs, respectively. The dynamics of the system is obtained assuming zero temperature by solving the $N_p$ equations of motion

$$m\ddot{\mathbf{r}}_i = -\nabla_i E(\{\mathbf{r}_i\}) - \eta\mathbf{v}_i + \mathbf{F}_{\text{ext}}, \tag{5}$$

where $\eta$ is a damping coefficient accounting for the dissipation of kinetic energy of the particles in the island into the substrate and $\mathbf{F}_{\text{ext}}$ is the external driving force. The equations have been solved numerically with an adaptive Runge-Kutta integrator of the fourth order. Throughout the paper, all results obtained within the 2D FK model are expressed in simulation units, i.e., as obtained directly from the simulations performed at our chosen parameters, without any further conversion. Distances are understood to be in units of $a$.

### B. Simulation protocols

We considered circular islands of increasing radius $R =$ 15–350, containing up to $N_p \simeq 3.8 \times 10^5$ particles. The starting configurations were generated adopting the following protocol. For each size we considered a set of starting angular orientations $\theta$ between the crystalline axis of the island and of the substrate. We explored values between 0 and 5°, which include the Novaco-McTague orientation $\theta_{\text{NM}}$ (≈2.5°, within the chosen parametrization) predicted to be energetically favorable in the limit of an infinite monolayer [28]. The positions of all particles in the islands were fully relaxed via damped dynamics described by the equations of motion (5) in the absence of external force. At each size we selected the relaxed configuration corresponding to the minimum value of the total energy. During relaxation, the islands tended to rotate from the initial orientation towards the optimal misalignment $\theta_{\text{opt}}$ that minimizes the energy. For the largest sizes considered, where edge effects are minimized, we observed $\theta_{\text{opt}} \approx \theta_{\text{NM}}$, as predicted by linear response theory [28].

The optimized configurations were used as starting points for the measurement of the static friction force $F_s$. The latter has been calculated using three different lateral loading configurations: edge loading, which mimics the sideway pushing and pulling by a tip of atomic force microscope (AFM), and a uniform driving, which can be realized when the slider is

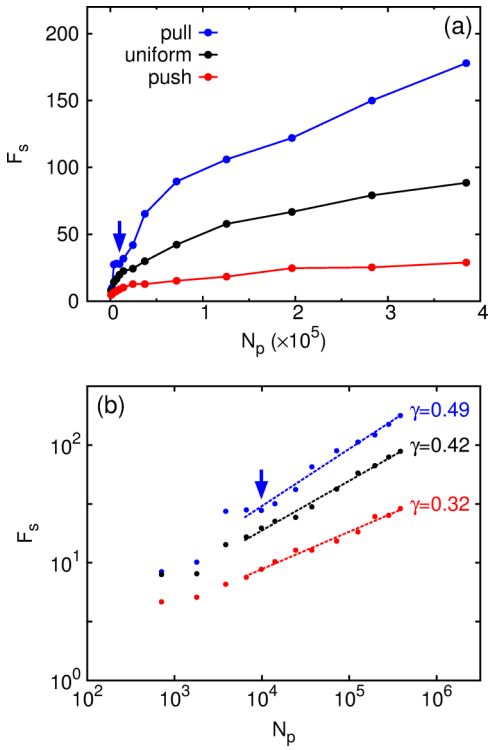


FIG. 2. (a) Size scaling of the static friction force. (b) A linear fit of the data in a log-log scale (dashed lines) yielded the scaling exponents $\gamma$ reported beside each curve. Blue, black, and red lines are results obtained under pulling, pushing, and uniform driving, respectively. Arrows indicate the critical size $N_p^*$ for the nucleation of a local commensurate dislocation in the case of pulling.

attached to a sufficiently rigid moving stage or subject to inertial forces as in quartz crystal microbalance experiments. To model the edge loading, we selected a small region at the edge of our islands comprising ∼70 particles, to which we apply the external force $F_{\rm ext}$ [see Fig. 1(b)]. A uniform driving is achieved applying $F_{\rm ext}$ to all particles. The static friction force is evaluated using an adiabatic protocol during which $F_{\rm ext}$ is increased in steps of $\Delta F = 0.0001$–$0.005$, much smaller than the single-particle depinning force $F_{s1} = \pi U_0/2\lambda_{\rm sub} \simeq 0.11$. For each value of $F_{\rm ext}$, the positions of all particles are relaxed via damped dynamics, using a damping $\eta = 0.5$. Depinning was detected by monitoring the displacement of the island's center of mass. We note that, as long as inertial effects are negligible during relaxation, the value of the static friction force is independent of the choice of the damping coefficient. To check the reliability of our protocol, we repeated some relaxations with the more sophisticated FIRE optimization algorithm [29], which yielded the same results. The data presented here were obtained applying the external force in the direction defined by $\theta_{\rm opt}$, corresponding to a high-symmetry lattice direction of the slider. We checked that the main results are qualitatively independent of the direction of application of the external force.

The applied external force induces strain deformations within the slider. These distortions occur mainly in the direction of the external force $F_{\rm ext}$, while the Poisson effect accounts for relatively smaller deformations in the perpendicular direction. We focus on the first, and we quantify them by

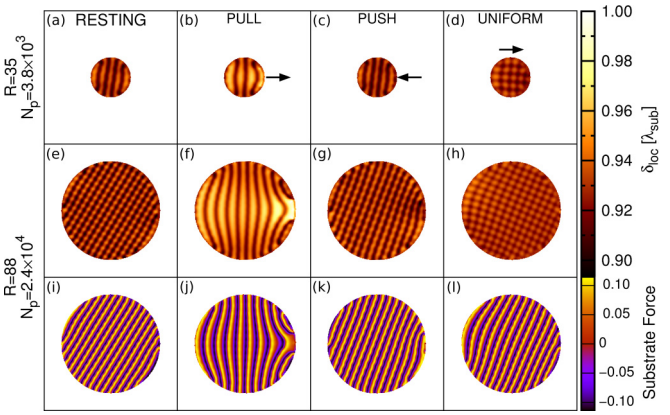


FIG. 3. (a)–(h) Colored maps showing the local mismatch $\delta_{\rm loc}$ of the circular islands in the 2D FK model simulations. Values of $\delta_{\rm loc} = 1$ indicate local commensuration to the substrate. Panels (a)–(d) show results for a size of $N_p \simeq 3.8 \times 10^3$ particles, while panels (e)–(h) correspond to $N_p \simeq 2.4 \times 10^4$. (i)–(l) Color maps of the substrate potential force (projected along the direction opposite to that of the external force) in the island of size $N_p \simeq 2.4 \times 10^4$. Positive values correspond to regions resisting the motion. Within the bulk, the substrate forces alternate in sign, summing up to nearly zero, and pinning originates mainly at the edges. From left to right, snapshots are shown obtained at rest [$F_{\rm ext} = 0$, panels (a), (e), (i)], and at an applied external force just below the static friction force value $F_{\rm ext} \lesssim F_s$ under edge pulling [panels (b), (f), (j)], edge pushing [panels (c), (g), (k)], and uniform driving [panels (d), (h), (l)]. Arrows indicate the direction of $F_{\rm ext}$ in the three protocols.

computing the local average distance $\delta_{\rm loc}(\mathbf{r}_i)$ of each particle $i$ from its nearest neighbors lying along the direction of the applied force. Two-dimensional color maps of $\delta_{\rm loc}$ are produced to gain insights on the driving-induced strain distribution. One-dimensional plots are extracted by averaging $\delta_{\rm loc}$ in the direction perpendicular to $F_{\rm ext}$, $\delta(x) = \langle \delta_{\rm loc}(\mathbf{r}_i) \rangle_\perp$. Both $\delta_{\rm loc}$ and $\delta$ are expressed in units of the substrate periodicity $\lambda_{\rm sub}$, so to easily detect local commensuration when $\delta_{\rm loc}/\lambda_{\rm sub} = 1$.

### C. Results: Size scaling and driving-induced elasticity effects

Figure 2, the main result of this study, reports the size dependencies of the static friction force calculated for three different lateral loading configurations: edge pulling, uniform driving, and edge pushing. We extract three main observations: (i) Static friction obeys a sublinear size scaling law, $F_s \propto N_p^\gamma$ with $\gamma < 1$, independent of the driving protocol [see Fig. 2(b)]. (ii) At all sizes we consistently observe $F_s^{\rm pull} > F_s^{\rm uniform} > F_s^{\rm push}$. The effect of nonuniform driving is indeed quite large: the static friction force measured for edge pulling being more than twice that obtained under uniform shearing, and almost one order of magnitude larger than the value measured for edge pushing. (iii) More surprisingly, the scaling exponent itself is found to depend significantly on the adopted lateral loading, and shows the same trend, $\gamma_{\rm FK}^{\rm pull} > \gamma_{\rm FK}^{\rm uniform} > \gamma_{\rm FK}^{\rm push}$, of the corresponding static friction force values.

To understand the physical origin of this behavior, we analyzed the preslip strain distribution at the interface. Figures 3(a)–3(h) report the colored maps of $\delta_{\rm loc}$ for two sizes, comparing the configurations at rest [$F_{\rm ext} = 0$, see Figs. 3(a)

and 3(e)] with the ones relaxed in presence of an external force just below the static friction threshold $F_{\rm ext} \lesssim F_s$ [see Figs. 3(b)–3(d) and 3(f)–3(h)]. At all sizes, the strain distribution is strongly dependent on the lateral loading. For the overdense case considered, pulling induces elongations of the interparticle distances in the direction of the applied external force, while pushing tends to reduce the bond lengths. In both cases, the largest distortions are localized near the edge region to which the external force is applied [see Figs. 3(b), 3(c), 3(f), and 3(g)]. A uniform shearing generally yielded mild compressions at the leading edge and somewhat larger elongations at the trailing edge [see Figs. 3(d), 3(h), and the full nearest-neighbor distances distributions reported in Fig. S2 of SM [27]]. Elasticity effects are particularly large for the edge-pulling protocol. There, as the size of the slider increases, the local bond length approaches values that grow closer and closer to the substrate periodicity $\delta_{\rm loc}/\lambda_{\rm sub} \to 1$ [see Figs. 3(b) and 3(f)].

In finite 2D superlubric contacts, locking to the substrate originates from lower-coordinated atoms that soften the slider at its border, hence, the static friction scaling is expected to increase at most as $\gamma_{\max} = \frac{1}{2}$. In our system, evidences of this behavior can be observed from the colored maps of the substrate forces acting on the slider [see Figs. 3(i)–3(l)]. In agreement with previous work [25] we actually found values of $\gamma < \frac{1}{2}$ [see Fig. 2(b)], indicating that pinning originates from a subset of points that grow sublinearly even with respect to the edge. Defining $F^*$ as the force needed to nucleate a localized commensurate dislocation, there must exist a corresponding threshold size $N_p^*$ above which $F^* \leqslant F_s(N_p)$ and local matching, namely, $\delta_{\rm loc}(\mathbf{r})/\lambda_{\rm sub} = 1$ for some $\mathbf{r}$, should occur before the onset of motion. We found that this is indeed the case, as demonstrated in Fig. 4. There, we show the average nearest-neighbor distance $\delta(x)$ measured along the direction of the external force, for two distinct island sizes. For $N_p = 3.8 \times 10^3 < N_p^* \approx 10^4$, the island is incommensurate everywhere, independent of the driving protocol. At $N_p = 2.4 \times 10^4 > N_p^*$, a localized commensurate dislocation is formed close to the pulling region. The same behavior was observed at each value of $N_p > N_p^*$, up to the largest size investigated. On the other hand, for edge pushing and uniform lateral loading, we found no evidence of nucleation of a commensurate dislocation, up to the largest value of $R = 350$ ($\sim 5\ b_{\rm core}$) considered. The emergence of commensurability is expected to affect the measured value of the static friction force, and indeed, for edge pulling we found a sharp increase just above $N_p \approx N_p^*$ [see arrow in Fig. 2(a)].

Coming to the scaling exponents, in Fig. 2(b) we report the results of a fit of the simulations' data. In our overdense contact, pushing promotes incommensurability by compressing the slider lattice spacing $a$. Correspondingly, we observed the smallest value of $\gamma_{\rm FK}^{\rm push} = 0.32 \pm 0.01$. The uniform shearing yielded an intermediate value $\gamma_{\rm FK}^{\rm uniform} = 0.42 \pm 0.01$, in agreement with the observation of more enhanced bond elongations, compared to compressions, taking place at the interface (see Fig. S2 of SM [27]). We note that a similar value of $\gamma^{\rm uniform} \approx 0.4$ was previously reported in atomistic simulations of circular Kr islands sliding on Pb(111) [25]. Finally, the largest value $\gamma_{\rm FK}^{\rm pull} = 0.49 \pm 0.02$ is obtained for edge pulling, reflecting

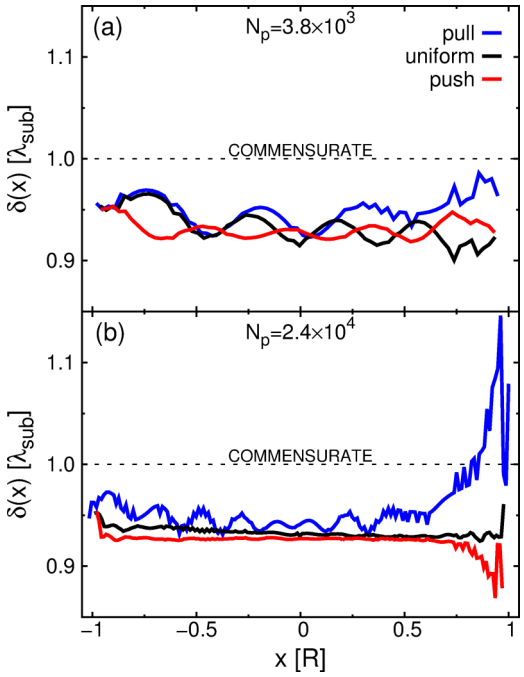


FIG. 4. The averaged local mismatch $\delta(x)$ inside the circular islands of the 2D FK model simulations. Values of $\delta(x) = 1$ indicate local commensuration to the substrate. Panels (a) and (b) show results for two islands' sizes of $N_p \simeq 3.8 \times 10^3$ and $N_p = 2.4 \times 10^4$ particles, corresponding to radii of $R = 35$ and 88, respectively. Blue, red, and black lines are obtained from the analysis of the configurations relaxed at an external force just below the static friction force $F_{\rm ext} \lesssim F_s$ under edge pushing, edge pulling, and uniform driving, respectively.

the pinning effect of the localized commensurate dislocation, that adds to the edge contribution [see also the force map of Fig. 3(j)].

It is worth stressing that despite the presence of a commensurate dislocation, $F_s$ obeys a sublinear scaling law even under edge pulling, indicating that the commensurate area does not grow linearly with the contact size. Thus, our simulations demonstrate that the emergence of a localized commensurate region is not incompatible with the observation of a static friction sublinear scaling, which is usually considered a fingerprint of superlubricity. This conclusion differs from that of the work by Sharp *et al.* [21], where, within a similar simplified elastic model under the uniform loading, a transition from a sublinear scaling to a linear scaling of $F_s$ has been predicted for the contact size corresponding to the appearance of commensurate dislocations. In that case, the linear scaling of $F_s$ is determined by the increase of the number of dislocations that can be stabilized at the (quasistatically) sliding interface [30]. It should be noted that, at least for some set of parameters, the results of simulations in Ref. [21] show the presence of localized commensurate dislocations already in the starting configurations at rest, suggesting that the contacts were not in the superlubric regime (see discussion in Sec. S1 of SM [27]). In our case, an externally applied nonuniform driving force is necessary for the appearance of a commensurate dislocation. Moreover, during sliding the dislocation remains localized near

the edge, and no others are nucleated across the contact (see Fig. S3 of SM [27]).

## III. ATOMISTIC MD SIMULATIONS

### A. Model: Au(111) over graphite

The comparative atomistic MD investigation deals with gold islands deposited on a graphitic substrate. We have considered Au(111) islands of circular shape [see Figs. 1(c) and 1(d)], fully described atomistically by embedded atom method (EAM) potential [31], with a spacing parameter $a = 4.63$ Å, and deposited on a graphene monolayer kept rigid in its bulk configuration, corresponding to a lattice constant $\lambda_{sub} = 4.26$ Å. Au-C interaction has been mimicked by a 12-6 Lennard-Jones potential, with $\epsilon = 44$ meV, $\sigma = 2.74$ Å, and a cutoff radius of 7Å. In order to reduce the critical island size at which its elasticity affects friction, we have used the same $\sigma$ but $\epsilon$ twice that of Lewis *et al.* [32]. We have considered Au island sizes with radii in the range $R = 6$–$40$ nm, the largest corresponding to about $8 \times 10^4$ Au atoms, adsorbed on a graphene sheet of $88 \times 88$ nm$^2$ ($\sim 3 \times 10^5$ C atoms) with applied periodic boundary conditions. The characteristic core width of interfacial edge dislocations for this system is of the order of $b_{core} \approx 18$ nm $= 39\ a$ (see Sec. S2 of SM [27]). After damped-dynamics relaxation we obtain an optimum alignment angle $\theta_{opt} \simeq 1.7^\circ$, as similarly observed in earlier work [33]. Dynamics was simulated using a velocity-Verlet integrator with a time step of 1 fs, and a viscous damping of $\eta = 0.1$ ps$^{-1}$. The protocols adopted for the initial relaxation and the subsequent measurement of the static friction force are the same as outlined in Sec. II B.

### B. Results: Interface strain distribution and size scaling

Contrary to the FK system, the existent mismatched ratio between gold and graphene defines an underdense contact geometry with $\lambda_{sub} < a$. Thus, adsorbate/substrate commensuration is expected to be favored by a sideways pushing instead of pulling. Figure 5 reports the colored strain maps for two island sizes and the different driving protocols previously considered, where close commensurate regions with the underneath substrate are highlighted by brighter tones.

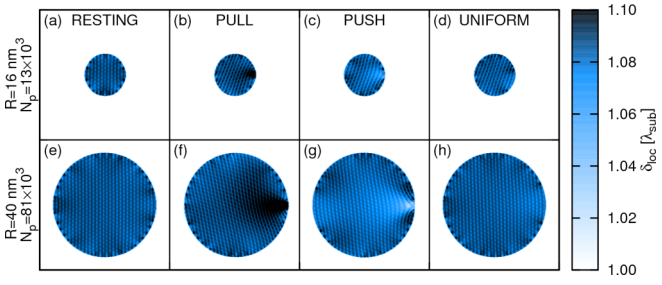


FIG. 5. Local mismatch maps for the gold-graphene system at two different island sizes $R = 16$ nm (a)–(d) and $R = 40$ nm (e)–(h). Aside from the resting (no external force) case, configurations for pulling, pushing, and uniform driving are reported with an applied force just below the depinning threshold. Local commensuration is achieved in the white region.

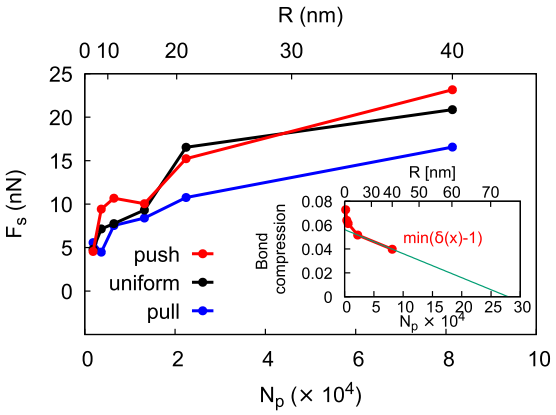


FIG. 6. Size scaling of the static friction force $F_s$ in the gold-graphene system. Blue, black, and red lines are results obtained during the pulling, uniform, and pushing protocols, respectively. The inset shows the scaling of the maximum bond compression during pushing. A linear extrapolation is used to obtain an approximate estimation of the critical size for the appearance of a local commensurate dislocation.

While the smaller adsorbate (top panels) does not exhibit significant strain deformations regardless of the type of applied shearing, the larger slider (bottom panels) starts to develop, under sideways pushing, the nucleation of a localized nearly commensurate zone.

Figure 6 reports the corresponding size scaling of the static friction force. We observe $F_s^{pull} < F_s^{push} \approx F_s^{uniform}$, indicating again that pinning to the substrate can be reduced by adopting lateral loading configurations that promote incommensurability. Under edge pushing and uniform driving, up to the largest size investigated, local commensuration is approached but never reached. Correspondingly, we measured comparable values of the static friction force, as similarly observed in the FK model well below $N_p^*$ [see Fig. 2(b)]. A tentative fit of the simulations' data (see Sec. S5 of SM [27]) yielded $\gamma_{gold}^{pull} = 0.33 \pm 0.06$, $\gamma_{gold}^{uniform} = 0.39 \pm 0.05$, and $\gamma_{gold}^{push} = 0.38 \pm 0.06$. In analogy with the FK model, we note that the scaling exponents follow qualitatively the same trend displayed by the corresponding values of the static friction force. Moreover, we found agreement between the values of $\gamma_{gold}^{pull} \approx \gamma_{FK}^{push}$ and of $\gamma_{gold}^{uniform} \approx \gamma_{FK}^{uniform}$. On the other hand, since local commensuration is never reached in the gold-graphene system under sideways pushing, we observe $\gamma_{gold}^{push} < \gamma_{FK}^{pull}$. A rough estimate of the critical size for the appearance of a commensurate dislocation in the gold islands is given in the inset of Fig. 6. There we show the size dependence of the minimum distance from achieving local commensuration, $\min[\delta(x) - 1]$, measured for the pushing protocol. A linear extrapolation indicates that commensurate dislocations should nucleate above a critical island size of $R \gtrsim 75$ nm. The numerical inspection of such computationally demanding limit goes beyond the scope of the study. Nevertheless, the close similarity of the strain maps of Fig. 5 with those of Fig. 3, and the differences between the values of the static friction force highlighted in Fig. 6 suggest that a similar boost in the static friction is to be expected in sufficiently large real contacts as well.

## IV. DISCUSSION AND CONCLUSIONS

We carried out a detailed numerical investigation of the static friction force $F_s$ arising in crystalline nanocontacts for three different lateral loading configurations. We focused on incommensurate superlubric interfaces, for which a sublinear scaling of $F_s \propto A^{\gamma<1}$ with respect to the contact area $A$ has been predicted theoretically [25,34], and observed experimentally [11,12]. Results obtained within the framework of a two-dimensional Frenkel-Kontorova model [35] demonstrate that both the absolute value $F_s$ and the scaling exponent $\gamma$ depend on the lateral loading configuration adopted to drive the slider along the substrate. Specifically, we observed variations of nearly one order of magnitude in the measured value of $F_s$ upon changing the direction of the applied shearing force during sideways pushing/pulling of circular islands. On top of that, the scaling exponent $\gamma$ itself was found to vary by $\sim$50%.

This behavior is tightly linked to the preslip strain distribution induced at the frictional interface. Larger (smaller) values of $(F_s,\gamma)$ are observed in concomitance of lateral loading configurations that stretch (compress) the slider lattice spacing $a$ towards (away from) matching with the periodicity $\lambda_{\text{sub}}$ of the underlying crystalline substrate. A large boost of static friction is observed when the contact area exceeds a critical value above which the static friction force becomes larger than the force $F^*$ needed to nucleate a localized commensurate dislocation near the driven edge. Remarkably, independent of the presence or absence of commensurate dislocations, the scaling law remains sublinear, indicating that the commensurate area does not increase proportionally to $A$. This result further demonstrates that a sublinear scaling, usually considered a fingerprint of superlubricity, does not conflict with the possibility to observe shear-induced localized commensurate regions at the contact interface. Comparative atomistic simulations of gold nanosliders deposited over a graphitic substrate corroborated these findings, thus suggesting that similar effects should be at play in sufficiently large real contacts that can be probed in nanomanipulation experiments [12].

We mention here that previous works [22,23] dealing with an edge-driven one-dimensional FK model reported the occurrence of a boost of energy dissipation above a critical length corresponding to the nucleation of a localized commensurate region. In that case, the threshold value was determined by the linear increase with contact size of the viscouslike kinetic friction force needed for attaining steady sliding at a given constant velocity. In superlubric one-dimensional contacts of increasing size, static friction instead oscillates around a constant value [36], hence, the creation of a commensurate dislocation before the onset of motion is hindered if $F_s < F^*$, which is generally the case. Again in connection with elasticity, in a recent work by Sharp *et al.* [21], a transition from a sublinear to linear scaling of $F_s$ has been predicted for the contact size corresponding to the appearance of interfacial commensurate dislocations characterized by a core width $b_{\text{core}}$. However, in that case the transition was observed only for the case of soft sliders, corresponding to small values of $b_{\text{core}}/a \lesssim 2$. Moreover, local commensuration was reported even in the absence of external shearing forces, suggesting that the contacts were not genuinely superlubric. On the contrary, the results of our simulations fall in the regime of stiff sliders and a large $b_{\text{core}}/a \gg 1$, where local commensuration is observed only under the action of a nonuniform lateral loading. The present investigation therefore highlights a mechanism for nucleation of edge-driving-induced commensurate dislocations which lead to a signicant increase of the static friction force, while remaining in a regime of sublinear scaling.

In our simulations, the external force $F_{\text{ext}}$ was applied to $N_{\text{driven}} \sim 70$ particles at the edge of the slider. More generally, the frictional response of the system will depend on the fraction $f_d = N_{\text{driven}}/N_p$ of driven particles. For a fixed size $N_p$ of the slider, under sideways pushing/pulling, the static friction force will tend to the uniform driving value, $F_s \to F_s^{\text{uniform}}$ for $f_d \to 1$, even though not necessarily in a continuous fashion. We can expect a similar scenario also for the scaling exponent. Increasing the fraction $f_d$ of driven particles will lead to a crossover of the scaling exponent $\gamma(f_d)$, from the nonuniform value at small fractions, to the uniform value at larger fractions, where the stress distribution becomes homogeneous. The way the uniform value is approached will depend on the details of the definition of the driven region.

Summarizing, while it has been shown that the static friction force scaling exponent $\gamma$ of incommensurate crystalline interfaces depends on the geometrical properties of the contact, including the shape of the slider and the mismatch and symmetry of the contacting lattices [25,34], our results prove that $\gamma$ can vary significantly due to elasticity effects. These, in turn, can be characterized in terms of the interfacial strain distribution induced by the externally applied shear stress. In particular, in sufficiently large contact geometry, the possibility that the edge-driving-induced nucleation of localized commensurate dislocations leads to the breaking of superlubric sublinear scalings cannot be excluded, and certainly deserves further investigation. Interestingly, variations of the static friction with the loading configuration has been found previously for elastic macroscopic contacts [37,38], where this effect results from changes in the rupture dynamics at the rough frictional interface.

## ACKNOWLEDGMENTS

D.M. acknowledges the fellowship from the Sackler Center for Computational Molecular and Materials Science at Tel Aviv University, and from the Tel Aviv University Center for Nanoscience and Nanotechnology. W.O. acknowledges the financial support from a fellowship program for outstanding postdoctoral researchers from China and India in Israeli Universities. M.U. acknowledges the financial support of the Israel Science Foundation Grant No. 1316/13. A.V. and R.G. acknowledge financial support by ERC Grant No. 320796 MODPHYSFRIC. COST Action MP1303 is also gratefully acknowledged.

[1] A. Vanossi, N. Manini, M. Urbakh, S. Zapperi, and E. Tosatti, Rev. Mod. Phys. **85**, 529 (2013).

[2] M. Urbakh, J. Klafter, D. Gourdon, and J. Israelachvili, Nature (London) **430**, 525 (2004).

[3] M. Urbakh and E. Meyer, Nat. Mater. **9**, 8 (2010).
[4] N. Manini, G. Mistura, G. Paolicelli, E. Tosatti, and A. Vanossi, Adv. Phys. X **2**, 569 (2017).
[5] M. Hirano, K. Shinjo, R. Kaneko, and Y. Murata, Phys. Rev. Lett. **78**, 1448 (1997).
[6] M. Dienwiebel, G. S. Verhoeven, N. Pradeep, J. W. M. Frenken, J. A. Heimberg, and H. W. Zandbergen, Phys. Rev. Lett. **92**, 126101 (2004).
[7] A. E. Filippov, M. Dienwiebel, J. W. M. Frenken, J. Klafter, and M. Urbakh, Phys. Rev. Lett. **100**, 046102 (2008).
[8] X. Feng, S. Kwon, J. Y. Park, and M. Salmeron, ACS Nano **7**, 1718 (2013).
[9] Z. Liu, J. Yang, F. Grey, J. Z. Liu, Y. Liu, Y. Wang, Y. Yang, Y. Cheng, and Q. Zheng, Phys. Rev. Lett. **108**, 205503 (2012).
[10] E. Koren, E. Lörtscher, C. Rawlings, A. W. Knoll, and U. Duerig, Science **348**, 679 (2015).
[11] D. Dietzel, M. Feldmann, U. D. Schwarz, H. Fuchs, and A. Schirmeisen, Phys. Rev. Lett. **111**, 235502 (2013).
[12] E. Cihan, S. Ipek, E. Durgun, and M. Z. Baykara, Nat. Commun. **7**, 12055 (2016).
[13] S. Kawai, A. Benassi, E. Gnecco, H. Söde, R. Pawlak, X. Feng, K. Müllen, D. Passerone, C. A. Pignedoli, P. Ruffieux, R. Fasel, and E. Meyer, Science **351**, 957 (2016).
[14] S. W. Liu, H. P. Wang, Q. Xu, T. B. Ma, G. Yu, C. Zhang, D. Geng, Z. Yu, S. Zhang, W. Wang, Y. Z. Hu, H. Wang, and J. Luo, Nat. Commun. **8**, 14029 (2017).
[15] M. Pierno, L. Bruschi, G. Mistura, G. Paolicelli, A. di Bona, S. Valeri, R. Guerra, A. Vanossi, and E. Tosatti, Nat. Nanotechnol. **10**, 714 (2015).
[16] T. Bohlein, J. Mikhael, and C. Bechinger, Nat. Mater. **11**, 126 (2012).
[17] A. Bylinskii, D. Gangloff, and V. Vuletić, Science **348**, 1115 (2015).
[18] A. Bylinskii, D. Gangloff, I. Counts, and V. Vuletić, Nat. Mater. **15**, 717 (2016).
[19] J. Kiethe, R. Nigmatullin, D. Kalincev, T. Schmirander, and T. E. Mehlstäubler, Nat. Commun. **8**, 15364 (2017).
[20] M. H. Muser, Europhys. Lett. **66**, 97 (2004).
[21] T. A. Sharp, L. Pastewka, and M. O. Robbins, Phys. Rev. B **93**, 121402(R) (2016).
[22] M. Ma, A. Benassi, A. Vanossi, and M. Urbakh, Phys. Rev. Lett. **114**, 055501 (2015).
[23] A. Benassi, M. Ma, M. Urbakh, and A. Vanossi, Sci. Rep. **5**, 16134 (2015).
[24] D. Dietzel, J. Brndiar, I. Štich, and A. Schirmeisen, ACS Nano **11**, 7642 (2017).
[25] N. Varini, A. Vanossi, R. Guerra, D. Mandelli, R. Capozza, and E. Tosatti, Nanoscale **7**, 2093 (2015).
[26] D. Dietzel, C. Ritter, T. Monninghoff, H. Fuchs, A. Schirmeisen, and U. D. Schwarz, Phys. Rev. Lett. **101**, 125505 (2008).
[27] See Supplemental Material at http://link.aps.org/supplemental/10.1103/PhysRevMaterials.2.046001 for more details regarding the models and the simulations' results.
[28] A. D. Novaco and J. P. Mc Tague, Phys. Rev. Lett. **38**, 1286 (1977).
[29] E. Bitzek, P. Koskinen, F. Gähler, M. Moseler, and P. Gumbsch, Phys. Rev. Lett. **97**, 170201 (2006).
[30] J. A. Hurtado and K.-S. Kim, Proc. R. Soc. London A **455**, 3385 (1999).
[31] R. A. Johnson, Phys. Rev. B **37**, 3924 (1988). The potential has been modified to have a smooth cutoff. Data tables are accessible at http://xmd.sourceforge.net/eam/uconn/au.txt
[32] L. J. Lewis, P. Jensen, N. Combe, and J.-L. Barrat, Phys. Rev. B **61**, 16084 (2000).
[33] R. Guerra, E. Tosatti, and A. Vanossi, Nanoscale **8**, 11108 (2016).
[34] A. S. de Wijn, Phys. Rev. B **86**, 085429 (2012).
[35] O. M. Braun and Y. Kivshar, *The Frenkel-Kontorova Model: Concepts, Methods, and Applications* (Springer, Berlin, 1998).
[36] L. Gigli, N. Manini, A. Benassi, E. Tosatti, A. Vanossi, and R. Guerra, 2D Mater. **4**, 045003 (2017).
[37] O. Ben-David and J. Fineberg, Phys. Rev. Lett. **106**, 254301 (2011).
[38] R. Capozza and M. Urbakh, Phys. Rev. B **86**, 085430 (2012).